

# New classification method of volcanic ash samples using statistically determined grain types

R. Noguchi<sup>1\*</sup>, H. Hino<sup>2</sup>, N. Geshi<sup>3</sup>, S. Otsuki<sup>3</sup>, and K. Kurita<sup>4</sup>

1. *Volcanic Fluid Research Center, School of Science, Tokyo Institute of Technology, 2-12-1, Ookayama, Meguro-ku, Tokyo 152-8551, Japan*
2. *Department of Computer Science, University of Tsukuba, 1-1-1 Tenoudai, Tsukuba, Ibaraki 305-8573, Japan*
3. *Geological Survey of Japan, AIST. AIST Build. No. 7, 1-1-1 Higashi, Tsukuba, Ibaraki 305-8567, Japan*
4. *Earthquake Research Institute, the University of Tokyo, 1-1-1 Yayoi, Bunkyo-ku, Tokyo, 113-0032, Japan*

\* Corresponding author: r-noguchi@ksvo.titech.ac.jp

# 1 abstract

2 We developed a method to classify volcanic ash samples by introducing statisti-  
3 cally determined grain types. Using more than 10,000 numbers of automatically  
4 measured grain data (parameters of grain shape and transparency) and the clus-  
5 ter analysis, we made grain types without human eyes. By components of the  
6 grain type in each samples, we classified samples from types of basaltic mono-  
7 genetic volcanoes: 1) Funabara scoria cone, Izu Peninsula, Japan (magmatic  
8 eruption origin); 2) Nippana tuff ring, Miyakejima, Japan (phreatomagmatic  
9 eruption origin); and 3) rootless cones in Myvatn, Iceland (rootless eruption ori-  
10 gin). We tested two cases; using grain shape parameters only, and both of grain  
11 shape parameters and transparency values. It is found that the sample clas-  
12 sification is more consistent with their eruption style in the case of using both  
13 parameters of grain shape and transparency. By sampling several layers of an out-  
14 crop, this procedure can be used to interpret changes in eruption/fragmentation  
15 style during a volcanic event. Furthermore, this procedure might be applicable  
16 to other aims such as sedimentology and planetary science.

## 17 1 Introduction

18 The grain morphology of volcanic pyroclasts provides important information that allows us  
19 to infer eruption styles and mechanisms from microscopic images of volcanic ash. Grain  
20 analysis can reveal the characteristics of magma vesiculation and subsequent fragmentation  
21 (e.g., [Heiken and Wohletz, 1985]). Several studies have attempted to parameterize grain  
22 shapes to explore possible relationships with their formation and fragmentation processes  
23 ([Dellino and La Volpe, 1996]; [Dellino et al., 2001]; [Maria and Carey, 2002]; [Maria and Carey, 2007];  
24 [Liu et al., 2015]; [Rausch et al., 2015]; [Schmith et al., 2017]).

25 Owing to recent developments of measurement instruments, we can easily parameterize

26 the visual characteristics (shape and luminance) of thousands of grains in a short time, and  
27 can perform quantitative analysis for large numbers of volcanic ash grains. Introducing an  
28 automated particle analyzer (APA), [Leibbrandt and Le Penec, 2015] tested several measure-  
29 ment procedures, before presenting an efficient measurement protocol for volcanic ash. In  
30 their system, the operating duration is 35 minutes for 5000 ash grains, and several shape  
31 parameters are measured for each ash grains.

32 When analyzing this type of multivariate data, the parameter selection step is essential.  
33 With this in mind, [Liu et al., 2015] used a cluster analysis to determine four optimal pa-  
34 rameters (solidity, convexity, axial ratio, and form factor), which can effectively account for  
35 the morphological variance of grains. [Maria and Carey, 2002, Maria and Carey, 2007] ap-  
36 plied the fractal spectrum technique to volcanic ash grains, and used the fractal values (they  
37 called as variables) to perform 1) cluster analyses for ash grains in each sample (consists of  
38 20 ash grains), and 2) principal component analyses for 140 of ash grains. Thus, we can use a  
39 combination of grain shape parameters and statistical techniques to determine eruption styles  
40 and characteristics from the analysis of volcanic ash. Although this approach has been shown  
41 to be effective, it remains necessary to verify the applicability of this procedure to wider data  
42 sets. Specifically, verification should involve simple eruption episodes, such as monogenetic  
43 eruptions. Furthermore, in comparison among samples, characteristics of magma such as  
44 chemical composition and phenocryst content should be considered.

45 When analyzing volcanic ash samples, there is a major problem; how to compare among  
46 samples. Field studies entail collecting many samples from several layers, outcrops, volcanic  
47 edifices, and volcanic systems. Sieving these samples to microscopic sizes involves several  
48 thousand ash grains. Many previous volcanic ash studies have focused on ash classification  
49 in one or limited numbers of samples. For sample classification, most previous studies have  
50 used one value for one parameter in one sample (e.g., [Dellino et al., 2001]); it far from  
51 traditional component proportion analysis under microscopic observation by human eyes,  
52 and made difficulty to its interpretation. In this background, we have to discriminate both

53 of volcanic ash grains and ash samples which comparable to microscopic observations.

54 In this study, we adopt cluster analyses for automatically-measured large volcanic ash  
55 datasets. Firstly we made "grain types" by quantitative grain parameters without human  
56 eyes, then classified samples using its proportion of each grain types. We construct a statis-  
57 tical analysis procedure for volcanic ash samples aimed 1) to compare samples from several  
58 layers, outcrops, volcanic edifices, and volcanic systems, and 2) to quantify the fragmentation  
59 degree and the effect of external water to volcanic explosions.

## 60 **2 Methodology**

### 61 **2.1 Prepared samples**

62 We use ash samples from non-altered monogenetic volcanoes to simplify the analysis. We col-  
63 lected 18 ash samples from three locations in Japan and Iceland (Table 1, Fig.S1,S2), which  
64 were formed during three different types of monogenetic eruption: magmatic (vaporization  
65 of volatiles in magma), phreatomagmatic (magma-water interaction), and rootless eruptions  
66 (explosive lava-water interaction). Since the chemical compositions and phenocryst char-  
67 acteristics (composition, mode, and size) of host magma have resemblances (Table 2), we  
68 selected ash samples from these three locations, and assumed that their phenocryst and  
69 magmatic features were the same. Each sample is composed of many ash grains, and the  
70 grain characteristics such as shape and size differ for each sample. The grain size distribution  
71 for each sample is shown in Fig.S3.

Table 1: List of samples used in this study. DRC: double rootless cone, SRC: single rootless cone.

Eruption type (sample location)	Sample ID	Number of grains	Note
Magmatic (Funabara, Izu Peninsula) Japan	FN15101201	131	Lower layer
	FN15101205	262	Upper than 01
	FN15101206	206	Upper than 05
	FN15101207	87	Upper than 06
	FN15101208	168	Upper than 07
Phreatomagmatic (Nippana, Miyakejima) Japan	NP15113001	1851	Lower layer
	NP15113002	707	Upper than 01
	NP15113003	428	Upper than 02
	NP15113004	1125	Upper than 03
	NP15113005	708	Upper than 04
	NP15113006	796	Upper than 05
	NP16102407	863	Upper than 06
Rootless (Myvatn, N Iceland) Iceland	MY13091004	923	DRC outer, middle layer
	MY13091006	1065	DRC inner, lower layer
	MY13091305	686	SRC, lower layer
	MY13091306	670	SRC, middle layer
	MY13091402	1479	SRC, upper layer, collected in Hagi
	MY13092002	965	SRC, lower layer

Table 2: Petrological information of samples used in this study.

	Magmatic Funabara	Phreatomagmatic Nippana (Miyakejima 1983)	Rootless Myvatn (Younger Laxa lava)
Bulk composition	SiO <sub>2</sub> 51.23 TiO <sub>2</sub> 1.09 Al <sub>2</sub> O <sub>3</sub> 17.3 Fe <sub>2</sub> O <sub>3</sub> 3.47 FeO 6.71 MnO 0.17 MgO 6.85 CaO 9.92 Na <sub>2</sub> O 2.71 K <sub>2</sub> O 0.41 H <sub>2</sub> O+ 0.4 H <sub>2</sub> O- 0.02 P <sub>2</sub> O <sub>5</sub> 0.28 Total 100.56	52.91 1.42 14.98 14.33 N/A 0.24 4.13 9.11 2.67 0.53 N/A N/A 0.14 100.46	49.3 1.1 14.98 0.9 9.27 0.19 6.96 12.63 2.15 0.91 0.79 0.00 0.28 99.46
Phenocrysts	olivine, pyroxene (augite and hypers- thene), quartz	plagioclase, clinopyrox- ene, magnetite	plagioclase, pyroxene, olivine
Mode of phe- nocrysts [%]	3.7%	5–8%: plagioclase, <0.1–0.3%: clinopyrox- ene, <0.2%: magnetite	less than 10%
Phenocrysts size	olivine: 1 mm, hypers- thene: <1 mm, quartz: 3 mm (occasionally), magnetite: 0.2 mm	plagioclase: 0.6–0.8 mm (major axes), 0.2– 0.3 mm (minor axes), clinopyroxene: 0.2–0.4 mm, magnetite: 0.2 mm	plagioclase: 0.2–0.6 cm (1.5–2 cm for large)
References	[Yusa and Kuroda, 1970]; [Hamuro, 1985]	[Fujii et al., 1984]; [Aramaki et al., 1986] (Sample ID: MYK-11)	[Thorarinsson, 1953]; [Höskuldsson et al., 2010]

### 72 2.1.1 Funabara scoria cone

73 Funabara scoria cone in Izu Peninsula (Fig.S1A) belongs to the Higashi-Izu monogenetic  
74 volcano group (HIMVG; [Koyama and Umino, 1991]). The monogenetic volcanic activity  
75 in HIMVG began in  $0.26 \pm 0.02$  Ma ([Hasebe et al., 2001]). Today, there are over 60 mono-  
76 genetic volcanoes in this area. This volcanic field displays a variety of magmatic compositions:

77 basaltic, andesitic, dacitic, and rhyolitic (e.g., [Hamuro, 1985]). The age of the Funabara sco-  
78 ria cone was estimated as  $0.20 \pm 0.08 - 0.22 \pm 0.09$  Ma by [Hasebe et al., 2001]. The rock type is  
79 basalt with 50.91–51.23 wt% of  $\text{SiO}_2$ , and the mode of phenocrysts is 3.7% ([Hamuro, 1985]).  
80 Currently, the Funabara scoria cone is being quarried, revealing a clear stratigraphic profile  
81 (Fig.2A). At the outcrop, we took five samples from bottom to top.

82 In  $2\phi$ – $3\phi$  scale, Funabara samples are dominant red-oxidized opaque grains (Fig.1). Under  
83 the incident lighting, they show glassy surface. They contains microlites (plagioclase, olivine,  
84 and magnetite) in microscopic observation ( $\times 500$  magnification). Some of them are coated  
85 with red-oxidized magna, therefore they are opaque in the transmitted lighting. Funabara  
86 samples also contain transparent grains: brownish yellow grains and free-crystals. Brownish  
87 yellow grains show glassy surface, and are more dominant in FN15101206. Free-crystals are  
88 plagioclase, olivine, and pyroxene.

### 89 **2.1.2 Nippana tuff ring**

90 Nippana tuff ring is a half-collapsed tuff ring in the south of Miyakejima Island, Japan  
91 (Fig.S1B). On October 3, 1983, explosive interactions of magma and sea water formed a  
92 tuff ring due to the eruption center reaching a littoral area on the southwestern flank of  
93 the main edifice of Miyakejima (Oyama) through a fissure vent system (e.g., [Sumita, 1985];  
94 [Aramaki et al., 1986]). The rock type is augite basalt with 52.3–54.6 wt% of  $\text{SiO}_2$ . and the  
95 mode of phenocrysts is less than 9% ([Aramaki et al., 1986]). After formation, the edifice  
96 was half destroyed by subsequent typhoons and erosion ([Sumita, 1985], Fig.2B). We collected  
97 seven samples at the outcrop from lower to upper layers.

98 Nippana samples are rich in transparent grains (Fig.1). Most of them are glass frag-  
99 ment which often contain microlites (plagioclase and magnetite) in microscopic scale ( $\times 500$   
100 magnification for  $2.5\phi$ – $3\phi$  grains). The others are free-crystals (plagioclase). NP16102407  
101 contains black opaque glassy grains. Qualitatively, characteristics of grain shapes are differ-  
102 ent among samples; inwardly convex shape (NP15113001, NP15113002, and NP15113003),

103 and rectilinear edge (NP15113004, NP15113005, and NP15113006).

### 104 **2.1.3 Myvatn rootless cones**

105 Myvatn is located in the north east of Iceland (Fig.S2). The volcanic activity around this  
106 area is part of the *Krafla Volcanic System*. In this volcanic system, most effusive lava is  
107 basaltic, with 49% wt% of SiO<sub>2</sub> ([Nicholson, 1990]). The mode of phenocrysts is less than 10%  
108 ([Höskuldsson et al., 2010]). In 2170±38 cal yr BP ([Hauptfleisch, 2012]), lava (*Younger Laxá*  
109 *lava*) erupted from fissure swarms 12 km long on the east side of the lake. The lava flowed  
110 over wetlands and the lake (old Lake Myvatn), and hundreds of rootless cones were formed  
111 by explosive interactions between the lava and lacustrine sediments ([Thorarinsson, 1979];  
112 [Einarsson, 1982]). Afterwards, the lava flowed down the Laxárdalur river, forming rootless  
113 cones, before reaching a northern bay. In [Höskuldsson et al., 2010], the duration of this  
114 eruption is estimated to have been 30 days from an analysis of the lava thickness based  
115 on an equation in [Hon et al., 1994]. Based on the microcrystalline growth data of olivine,  
116 [Dolvik, 2007b] gives the timing of the rootless eruption as 1–2 days after the start of this  
117 eruption. Some rootless cones have smaller cones inside of the summit crater (double rootless  
118 cones, DRCs, Fig.3; [Noguchi et al., 2016]), though typical ones have simple conical edifice  
119 (single rootless cones, SRCs). We collected samples from rootless cones in several areas  
120 of Myvatn (Fig.S2). MY13091004–MY13091006 and MY13091305–MY13091306 were taken  
121 from same cone, respectively (Fig.3, S4). MY13091402 was sampled in Hagi, 45 km distant  
122 from the fissure vents.

123 Most of grains in Myvatn samples are glassy (Fig.1). In transparent glassy grains, there  
124 found microlites (plagioclase). Plagioclases are also contained as free-crystals. There exist  
125 dappled grains. In the transmitted lighting, transparent grains are dominant in MY13091004  
126 and MY13091305, and opaque grains are rich in MY13091306 and MY13091402, qualitatively.



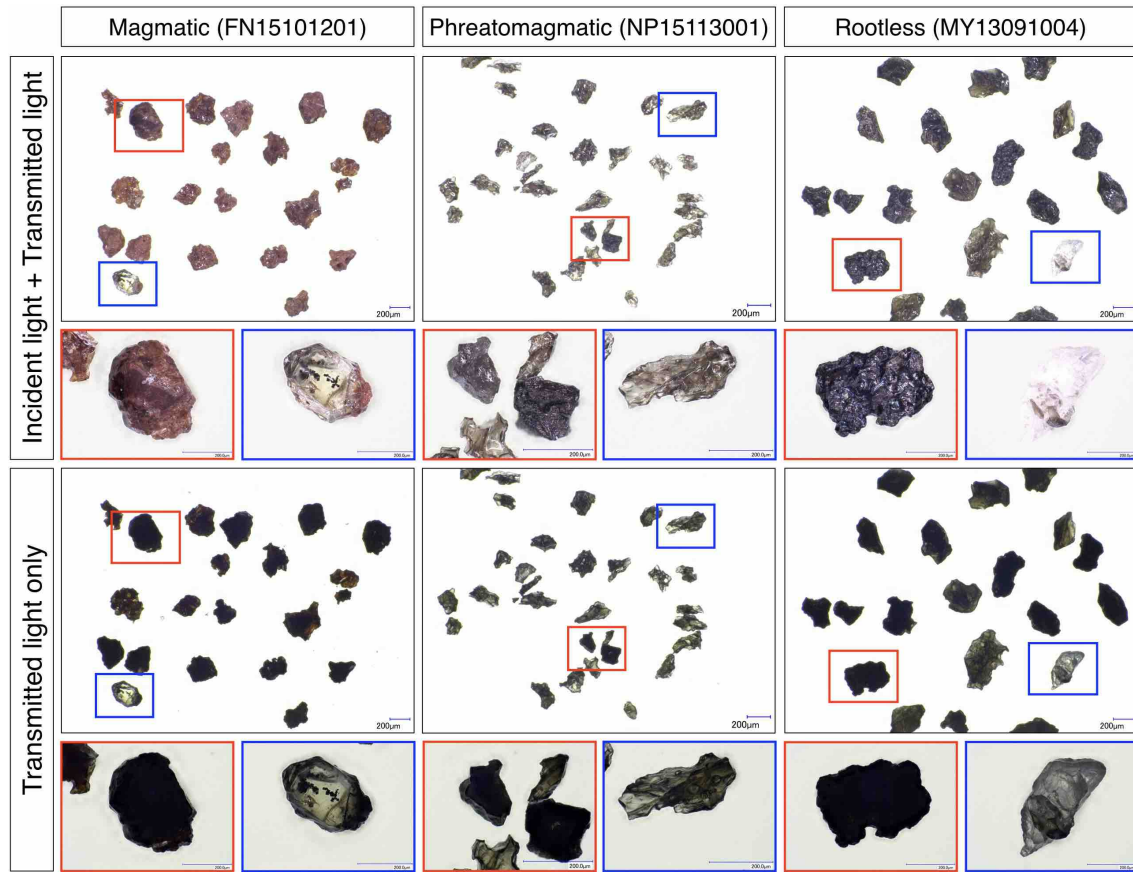


Figure 1: Examples of microscopic pictures of volcanic ash samples in this study. Red and blue boxes show example opaque and transparent grains, respectively. In the setting of the incident light + the transmitted light, the transmitted light is used to reduce shadow of grains. These microscopic pictures were taken by VHX-2000, KEYENCE at AIST.

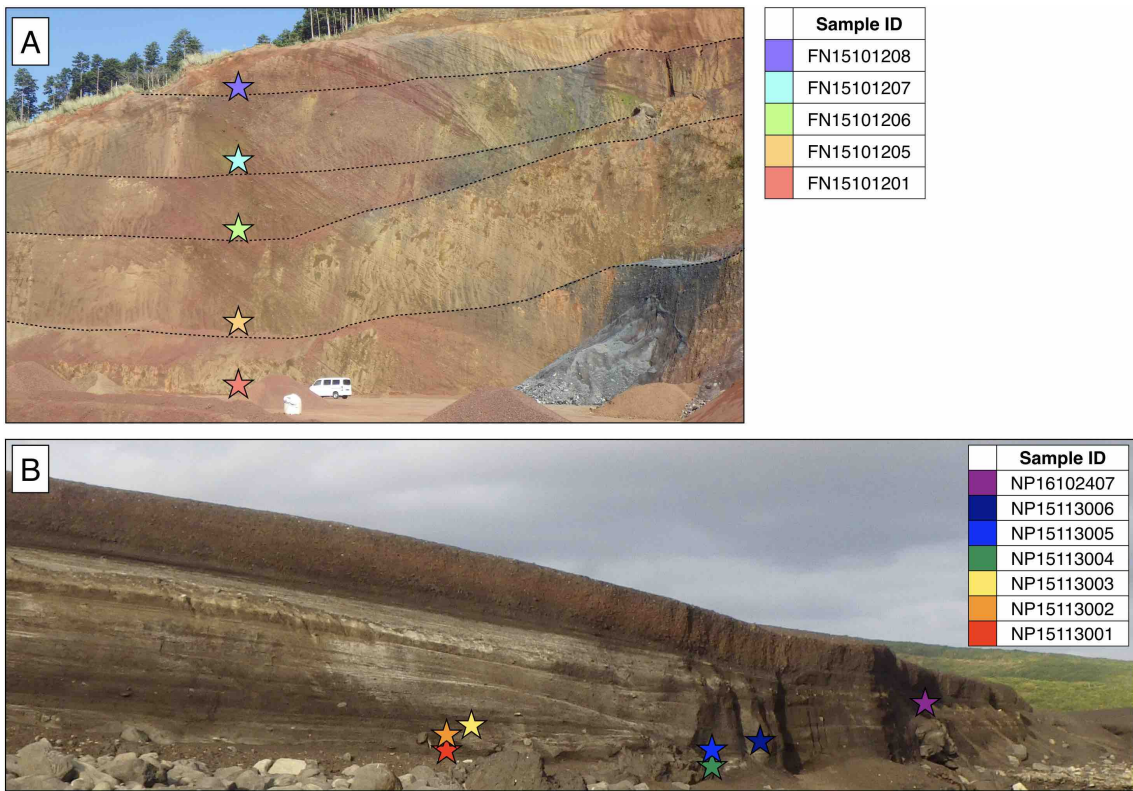


Figure 2: Sampling outcrops of Funabara scoria cone (A) and Nippana tuff ring (B).

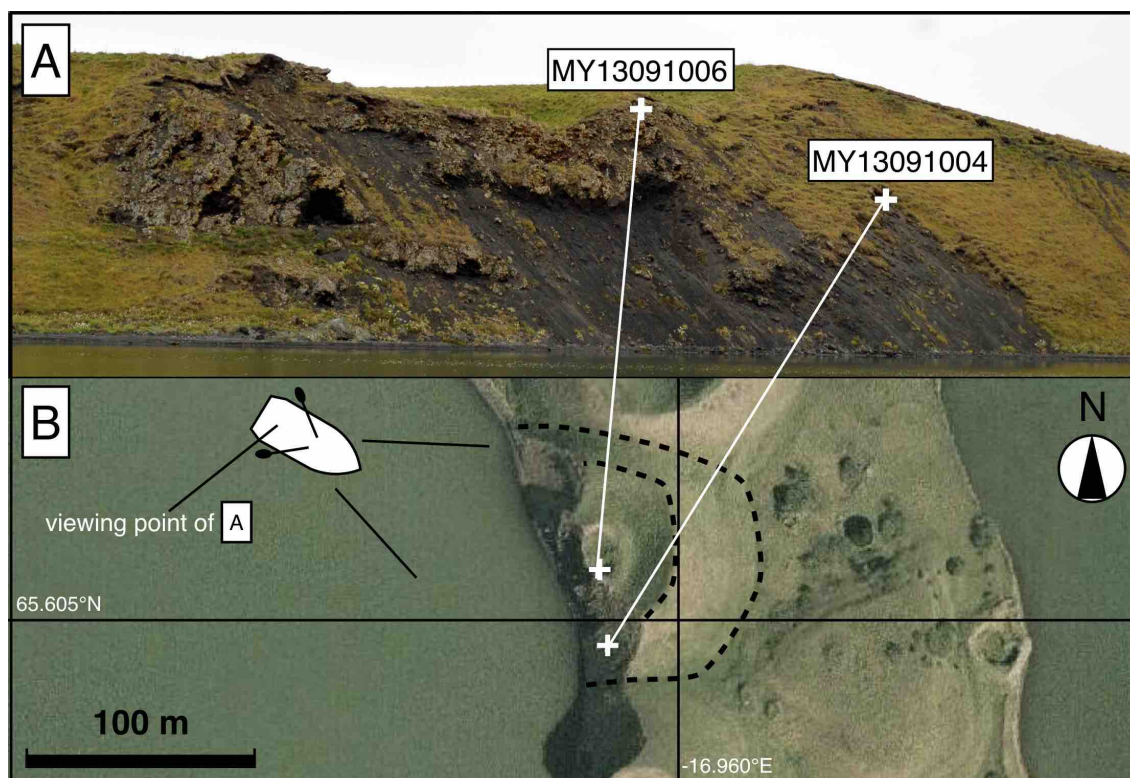


Figure 3: Sampling outcrops of Myvatn rootless cones for MY13091004 and MY13091006. This is a profile of double rootless cones which is thought to be formed by two stages of rootless eruptions ([Noguchi et al., 2016])

## 127 **2.2 Grain shape and transparency measurement**

128 The grain shape parameters of the pyroclasts were measured using an APA: Morphologi  
129 G3S<sup>TM</sup>(Malvern Instrument<sup>TM</sup>) at the Geological Survey of Japan, AIST. The detailed mea-  
130 surement method is shown in [Leibrandt and Le Penneç, 2015]. This study measured sieved  
131 volcanic ash grains ( $2.5\phi$  to  $3\phi$  fraction ( $160\mu\text{m}$  to  $250\mu\text{m}$ ) for Nippana samples (except  
132 NP16102407), and  $2\phi$ – $3\phi$  ( $125$ – $250\mu\text{m}$ ) for the others) at  $\times 5$  magnification. At this mag-  
133 nification, the measurable grain diameter ranges from  $6.5$  to  $420\mu\text{m}$ ; therefore, our sample  
134 sizes are appropriate for these measurement conditions. To place the volcanic ash grains on  
135 the glass plate, we used a Sample Dispersion Unit (SDU) with  $1.5$  bar of injection pressure  
136 and a  $20$  ms injection time. During the measurement, the illumination was set to diasopic  
137 (bottom light), under automatic light calibration (calibration intensity of  $80.00$  and intensity  
138 tolerance of  $0.20$ ). The threshold for background separation ( $0$ – $255$ ) was set at  $80$  to obtain a  
139 sharp focus. The measurement lasted approximately  $40$  min for each sample. After the mea-  
140 surement, we excluded overexposed, unseparated, and cut-off grains. To remove unwanted  
141 material (such as dust), we picked out grains with a solidity (a parameter of grain shape,  $S_d$ ,  
142 sensitive to morphological roughness; [Liu et al., 2015]) lower than  $0.6$ . In total, we collected  
143 parameterized data of  $13,120$  volcanic ash grains from the  $18$  samples.

## 144 **2.3 Grain parameters**

145 We used two-dimensional (2-D) projected images of ash grains to describe particle charac-  
146 teristics. Using Morphologi, we can obtain seven grain shape parameters (circularity, high  
147 sensitive circularity, convexity, solidity, aspect ratio, and elongation) and two transparency  
148 values (intensity mean and intensity standard deviation). [Liu et al., 2015] described four  
149 shape parameters: convexity, solidity, axial ratio, and a form factor (HS circularity in Mor-  
150 phologi), which they adopted for grain shape analyses of volcanic ash. In this study, we used  
151 the aspect ratio instead of the axial ratio, as it is not provided by Morphologi.

152 As well as grain shape, Morphologi can also measure luminance, which, under bottom

153 lighting conditions, indicates grain transparency. Information regarding the grain trans-  
 154 parency of volcanic ash is important for identifying the glass and crystal components; how-  
 155 ever, most previous research has focused on grain shape alone, with the exception of [Miwa et al., 2015].

156 In this analysis, we chose six parameters: aspect ratio ( $A_r$ ), convexity ( $C_v$ ), solidity ( $S_d$ ),  
 157 HS circularity ( $H_c$ ), intensity mean ( $I_m$ ), and the standard deviation of the intensity ( $I_{sd}$ ).  
 158 Derivations of these parameters are given by

$$A_r = \frac{W}{L}$$

$$C_v = \frac{P_c}{P_g}$$

$$S_d = \frac{A_g}{A_g + A_c}$$

$$H_c = \frac{4 \times \pi \times A_g}{P_g^2}$$

$$I_m = \frac{\sum_{i=1}^{i=N} I_i}{N}$$

$$I_{SD} = \sqrt{\frac{\sum_{i=1}^{i=N} I_i^2 - \frac{\left(\sum_{i=1}^{i=N} I_i\right)^2}{N}}{N}}$$

159 where  $W$  is length along the minor axis of the grain,  $L$  is length along the major axis  
 160 of the grain,  $P_c$  is perimeter of the convex hull,  $P_g$  is the perimeter of the grain,  $A_c$  is area  
 161 of the convex hull,  $A_g$  is the area of the grain,  $I_i$  is the intensity values (0–255) of pixel  
 162 ( $i$ ), and  $N$  is the total number of pixels in the grains ([Malvern Instruments Ltd, 2013]).

163 These parameters were calculated for each ash grain. Definitions for each morphometrical  
 164 parameter are shown in Fig.4.

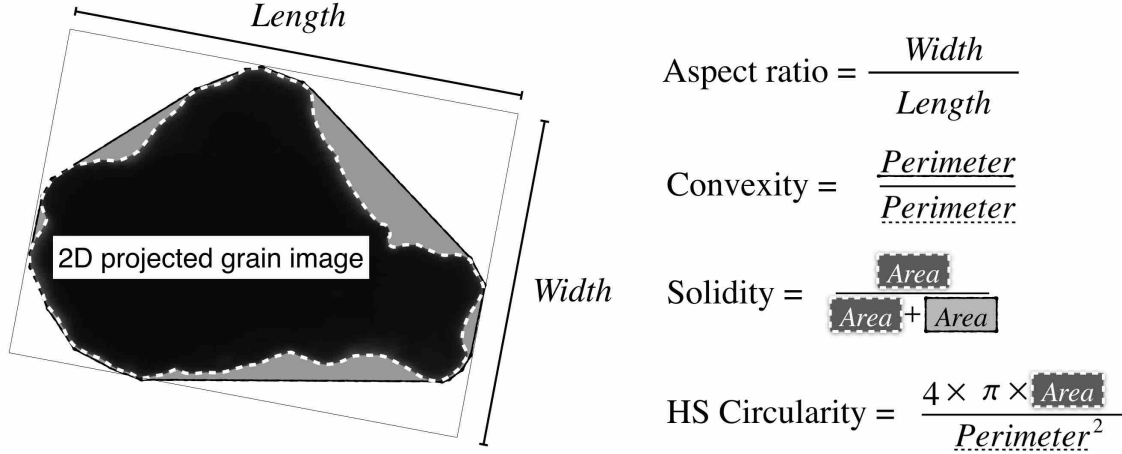


Figure 4: Derivations of grain shape parameters used in this study.

## 165 2.4 Data analysis

166 A standard cluster analysis technique ([Anderberg, 2014]) was applied to objectively and  
 167 quantitatively classify samples. The cluster analysis is one of the multivariate analysis method  
 168 for unsupervised classification. This statistical method is used in variety of fields such as mar-  
 169 keting research and machine learning. Using the cluster analysis, it is able to categorize data  
 170 quantitatively (based on the cluster distance such as the Euclidean distance) and visually (as  
 171 a dendrogram, a kind of tree diagram). In this study, we adopted the hierarchical clustering  
 172 method known as Ward’s method ([Anderberg, 2014]), because of its wide use and the ease  
 173 of clustering result interpretation. To apply the cluster analysis, we used standard machine  
 174 learning and statistical methods to compare samples, namely, we represented the grains and  
 175 samples by vectors composed of small number of features. Feature vector representation of  
 176 samples is convenient because we can use conventional methods of measuring the difference  
 177 between samples, i.e., the Euclidean distance between feature vectors of different samples.  
 178 The cluster analysis was performed using the `hclust` function equipped with the statistical

179 computing environment R ([R Core Team, 2016]).

180 To obtain the feature vector representation, we performed a two-step clustering analysis  
181 to 1) categorize whole ash into a small number of grain types, and 2) represent samples by a  
182 feature vector composed of the ash ratio (Fig.5). In the first cluster analysis, we categorized  
183 whole ash grains across the entire sample, and then considered each cluster as a statistically  
184 determined grain type. After calculating the grain number percentages of each grain type for  
185 all samples, considering the proportions of grain types as the feature vector for the sample,  
186 we then categorized the samples. We performed two sets of analyses, either including or  
187 excluding transparency values (i.e.,  $I_m$  and  $I_{sd}$ ), to evaluate the effect of transparency on  
188 our results. Because the range of values differ between shape parameters (0–1) and intensity  
189 values (0–255), ash grain data were standardized (using the `scale` function, with a mean 0  
190 and a standard deviation 1) before the analysis. Whole ash grain data include images are  
191 shown in the Supplemental Information.

192 To define grain types, we determined the number of clusters of whole ash grains in the  
193 samples. There are several methods for determining the number of clusters; for example,  
194 the R package `NbClust` provides 30 different indices for determining the number of clusters  
195 ([Charrad et al., 2014]). In the case of the `NbClust` package, the best number of clusters is  
196 determined by majority vote of the optimal numbers of clusters which are defined for each  
197 index based on maximum/minimum differentiation (see [Charrad et al., 2014] for details).  
198 Some of these indices require a heavy computational burden, particularly considering that  
199 our data includes 13,120 ash grains. In this case, it is recommended by the package authors  
200 to use only 18 of the 30 indices, which is more computationally efficient and do not depend on  
201 visual inspection. Therefore using `NbClust` package, we determined the appropriate cluster  
202 number for 13,120 ash grains. We analyzed both cases of including or excluding transparency  
203 values. See [Charrad et al., 2014] for details of the indices used in this study.

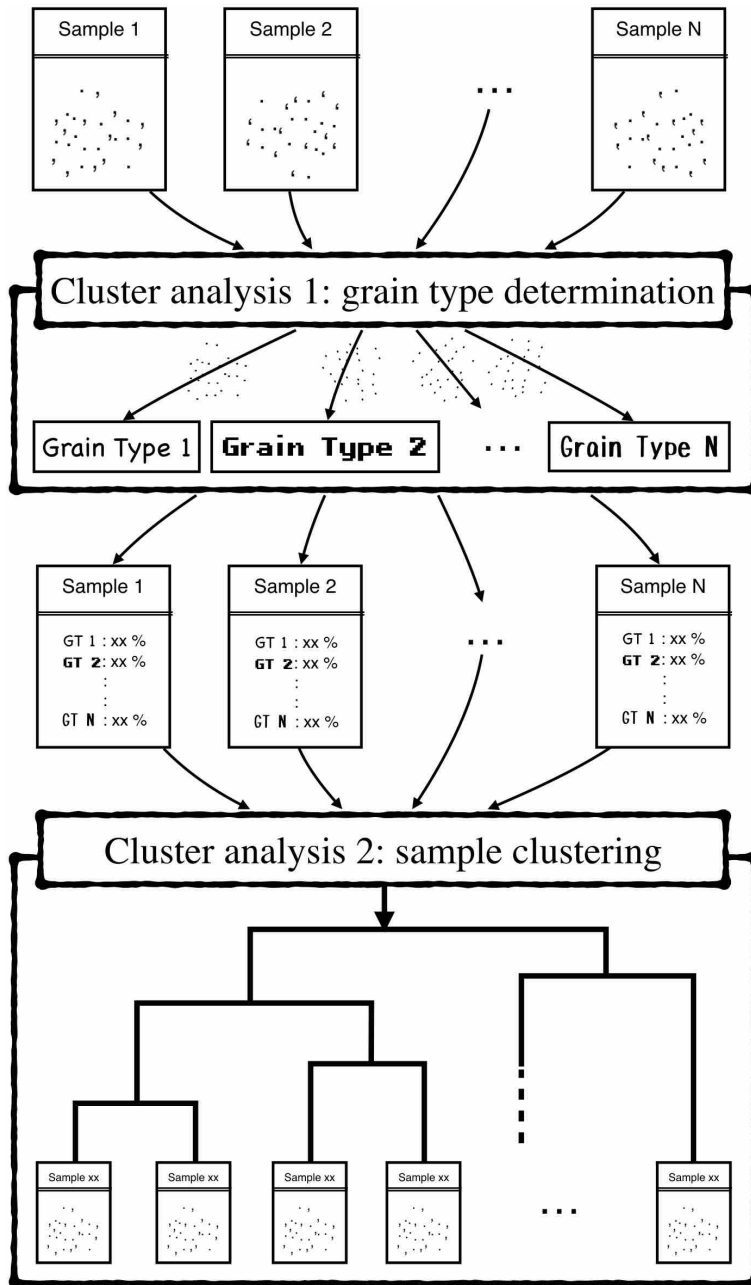


Figure 5: Cluster analysis procedure used in this study.



### 204 3 Results

205 We found that there is significant difference in the sample clustering results depending on  
206 whether transparency values are used or not. In the case of using transparency values, we  
207 got a consistent result of the sample clustering with their origin.

#### 208 3.1 Number of grain types

209 According to results of the `NbClust` analysis, the appropriate number of grain type was  
210 determined as two (Fig.6) for our dataset. Regardless of whether transparency values are  
211 used, the majority of indices showed their best number of clusters (`Best.nc` values in the  
212 `NbClust` package) as two. We checked and compared the results with the expectation of  
213 finding a larger number of grain type, but the results were almost equal. Therefore, the  
214 following analyses used two as the number of grain type.

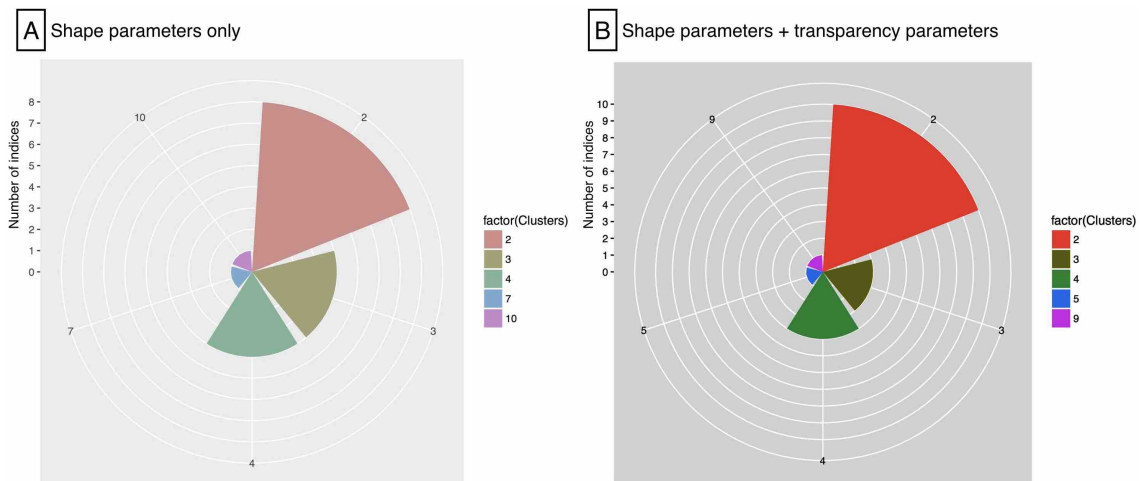


Figure 6: The appropriate number of grain type by the `NbClust` analyses. A: in the case of using grain shape parameters only. B: in the case of using grain shape parameters and transparency values. The radius of the pie chart shows the number of indices. Each color correlate with the number of clusters.

## 215 **3.2 Cluster analysis 1: grain type determination**

### 216 **3.2.1 I: grain shape only (without transparency values)**

217 Grains are divided into two clusters: an irregular-shape type (GT1) and a simple-shape type  
218 (GT2). Figs. 7A and B show the dendrogram and radar chart of centroids for each grain  
219 type. In the grain type determination, the aspect ratio is less effective, and others contribute  
220 to the classification (Fig.9). The larger cluster, GT2, includes 9,324 grains, and the smaller  
221 cluster, GT1, has 3,796 grains (Fig. 7). GT1 shows low values for all parameters, indicating  
222 irregular shape characteristics. GT2 generally shows high values, indicating rounded and  
223 smooth shape characteristics. Typical images of grains in each grain type are shown in  
224 Fig.10A.

### 225 **3.2.2 II: grain shape and transparency**

226 Grains are classified into two grain types: a simple-shape opaque type (GT3) and an irregular-  
227 shape transparent type (GT4) (Fig. 8). As is the case in 3.2.1, the aspect ratio does not show  
228 significant difference between these two grain types. GT3 includes 10,002 grains, and has the  
229 highest values of the four grain shape parameters, which indicate a relatively rounded and  
230 smooth appearance. The transparency values of GT3 grains are low, indicating its opacity.  
231 GT4, which includes 3,118 grains, has the lowest values of the four grain shape parameters,  
232 suggesting irregular grain shapes. Grains assigned to GT4 are transparent, as suggested by  
233 their higher transparency values. Typical images of grains in each grain type are shown in  
234 Fig.10B.

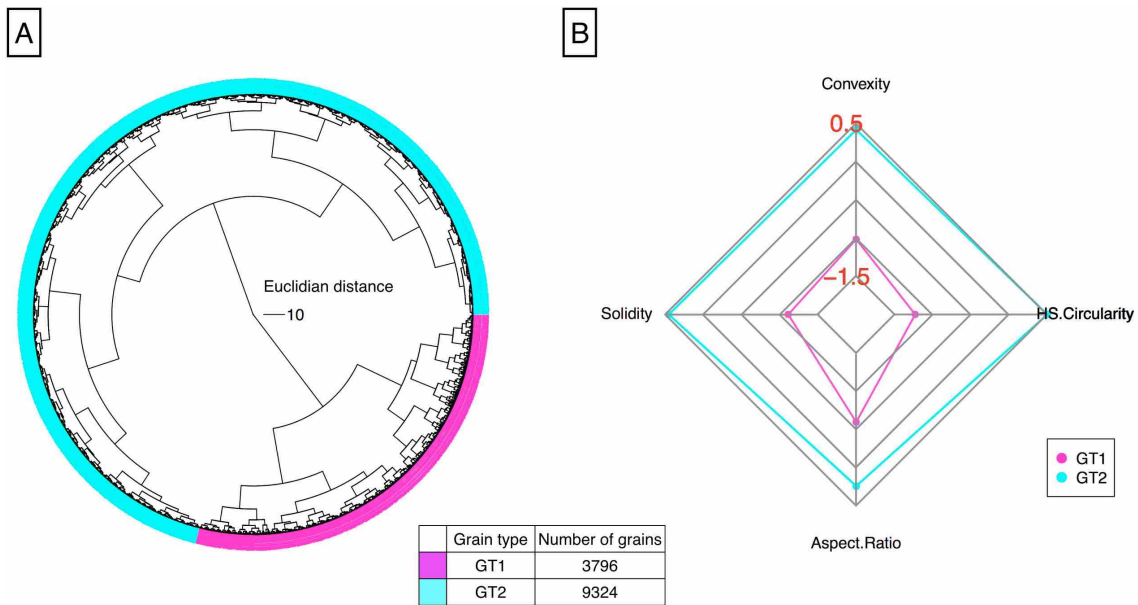


Figure 7: Results of cluster analysis 1: grain type determination. A : dendrogram for each grain type, and D: radar chart for each grain type.

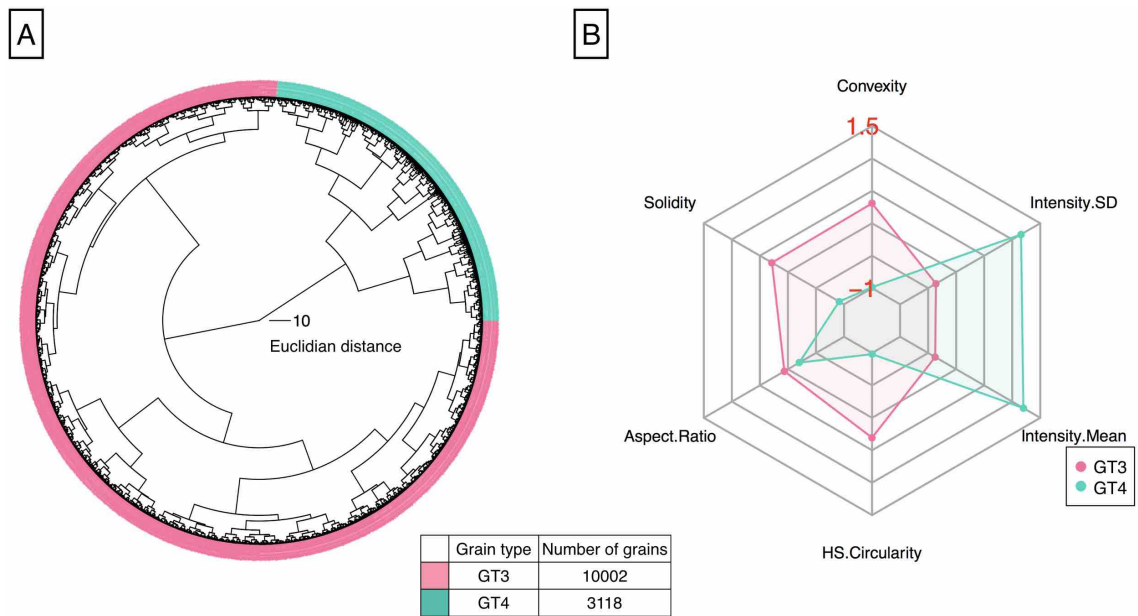


Figure 8: Results of cluster analysis 1: grain type determination. A : dendrogram for each grain type, and D: radar chart for each grain type.

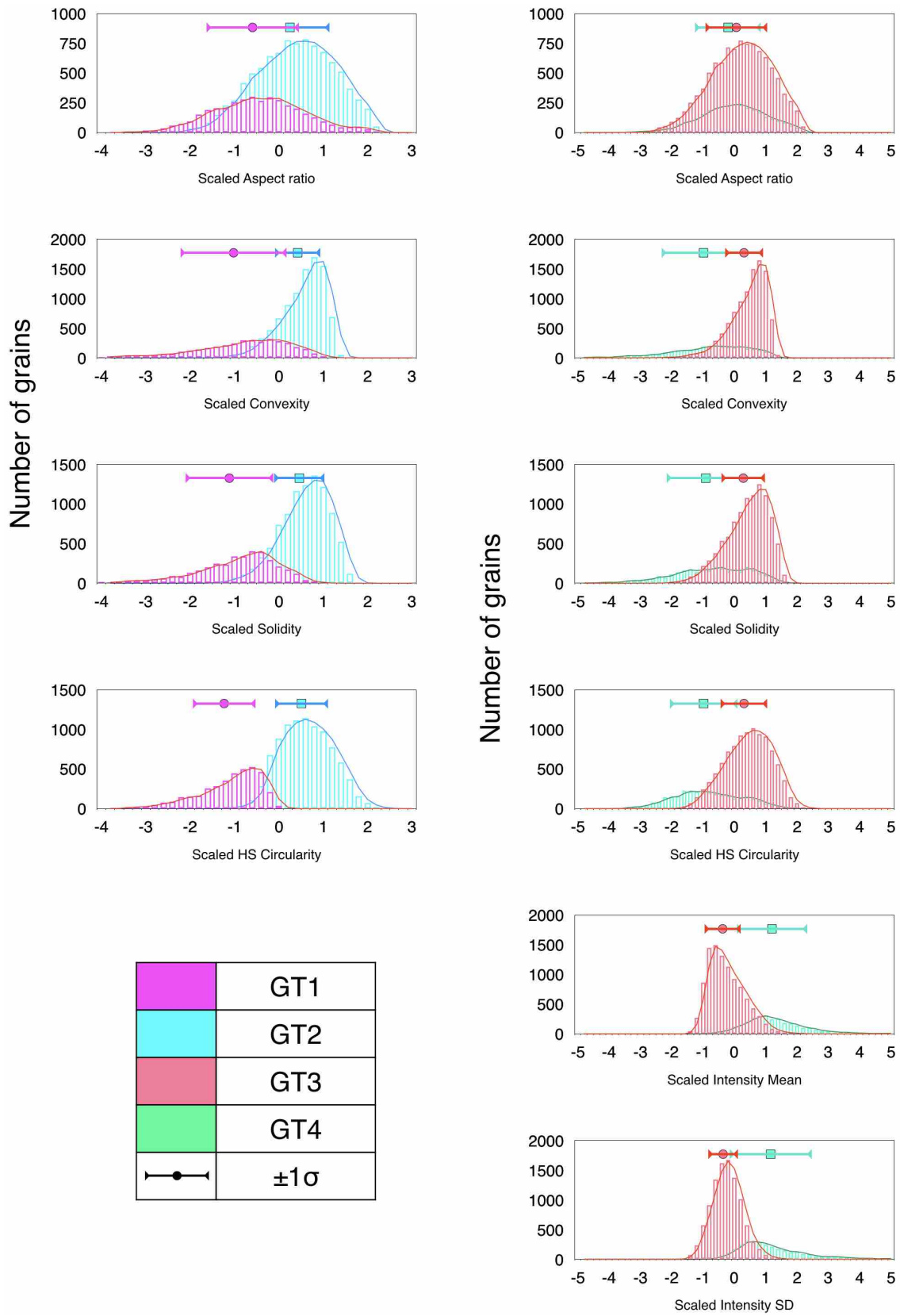




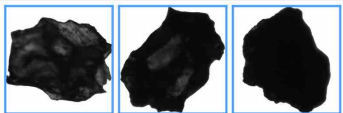



Figure 9: Histograms for each scaled parameters in cluster analysis 1. Left: shape parameters only. Right: shape parameters and transparency values.

**A** Shape parameters only

	Magmatic (FN15101201)	Phreatomagmatic (NP15113001)	Rootless (MY13091004)
GT1			
GT2			

**B** Shape parameters + transparency parameters


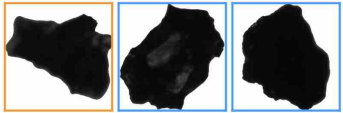


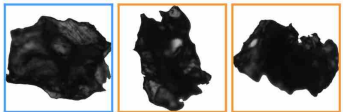

	Magmatic (FN15101201)	Phreatomagmatic (NP15113001)	Rootless (MY13091004)
GT3			
GT4			

Figure 10: Examples of grains in cluster analysis 1 for each grain type. Orange and blue boxed grains are determined as GT1 and GT2, respectively.

### 235 **3.3 Cluster analysis 2: sample clustering**

236 Percentage of numbers of grains in each grain type was calculated for every sample (Table  
237 3).

238 Components of GT1 grains reached 50 % only for NP15113001, NP15113002, and NP15113003.  
239 GT2 grains are dominant (over 80 %) for FN15101206, FN15101208, NP16102707, MY13091004,  
240 MY13091306, MY13091402, and MY13092002.

241 Funabara samples, MY13091006, MY13091306, and MY13091402 has significantly high  
242 component of GT3 grains (more than 90 %). NP15113001, NP15113002, and NP15113003  
243 has more than 50 % of components for GT4 grains.

244 Based on the proportions of grain types, we performed a cluster analysis for 18 samples  
245 from three origins.

Table 3: Grain type proportions for each sample.

Sample ID	GT1 [%]	GT2 [%]	GT3 [%]	GT4 [%]
FN15101201	32.82	67.18	93.13	6.87
FN15101205	26.72	73.28	95.04	4.96
FN15101206	14.56	85.44	97.09	2.91
FN15101207	28.74	71.26	97.7	2.3
FN15101208	11.31	88.69	100	0
NP15113001	50.62	49.38	43.92	56.08
NP15113002	51.06	48.94	49.79	50.21
NP15113003	53.04	46.96	50	50
NP15113004	23.82	76.18	73.33	26.67
NP15113005	34.32	65.68	68.36	31.64
NP15113006	25.88	74.12	71.61	28.39
NP16102407	14.95	85.05	86.67	13.33
MY13091004	19.83	80.17	88.84	11.16
MY13091006	22.16	77.84	93.62	6.38
MY13091305	38.92	61.08	67.06	32.94
MY13091306	16.87	83.13	92.39	7.61
MY13091402	18.66	81.34	95.33	4.67
MY13092002	16.89	83.11	89.74	10.26

### 246 3.3.1 I: Proportions of GT1 and GT2 grains (based on 3.2.1)

247 Using parameterized grain shape only results in poor correlation of sample classification  
248 with its origins (Fig. 11A). For example, FN15101201, NP15113005, and MY13091305 are  
249 classified similarly, yet they have different origins. An exception is samples NP15113001,  
250 NP15113002, and NP15113003, which have the same origin (collected in Nippana) and  
251 are well-categorized due to their higher components of GT1 grains (more than 50 %).  
252 MY13091004, MY13091006, and MY13091402 are relatively well-categorized, though with  
253 NP15113004 from the other origin.

### 254 3.3.2 II: Proportions of GT3 and GT4 grains (based on 3.2.2)

255 Samples from Funabara scoria cone and Nippana tuff ring are clearly distinguished when con-  
256 sidering both grain shape and transparency (Fig. 11B). The dominant component of the Fun-

257 abara samples is GT3 grains (more than 90 %, Fig. 11D, Table 3). Especially, FN15101206,  
258 FN15101207, and FN15101208, upper layers of Funabara samples, are categorized simi-  
259 larly due to their significantly high GT3 grain components. For samples from Nippana,  
260 the stratigraphically lower samples (NP15113001, NP15113002, and NP15113003) are split  
261 equally between GT3 and GT4, whereas the stratigraphically upper samples (NP15113004,  
262 NP15113005, NP15113006, and NP16102407) are richer in GT3 grains (over 68 %). In the  
263 dendrogram, NP16102407 was distinguished from other Nippana samples because its com-  
264 ponent of GT4 grains is low (13.3 %). Myvatn samples are dominant in GT3 grains (over  
265 65 %), however they were not categorized together. Notably MY13091305 was categorized  
266 within Nippana sample dominant cluster due to its higher component of GT4 grains (32.9  
267 %). Although they were collected from same rootless cone respectively, MY13091004 and  
268 MY13092002 are distinguished with MY13091006 and MY13091306.



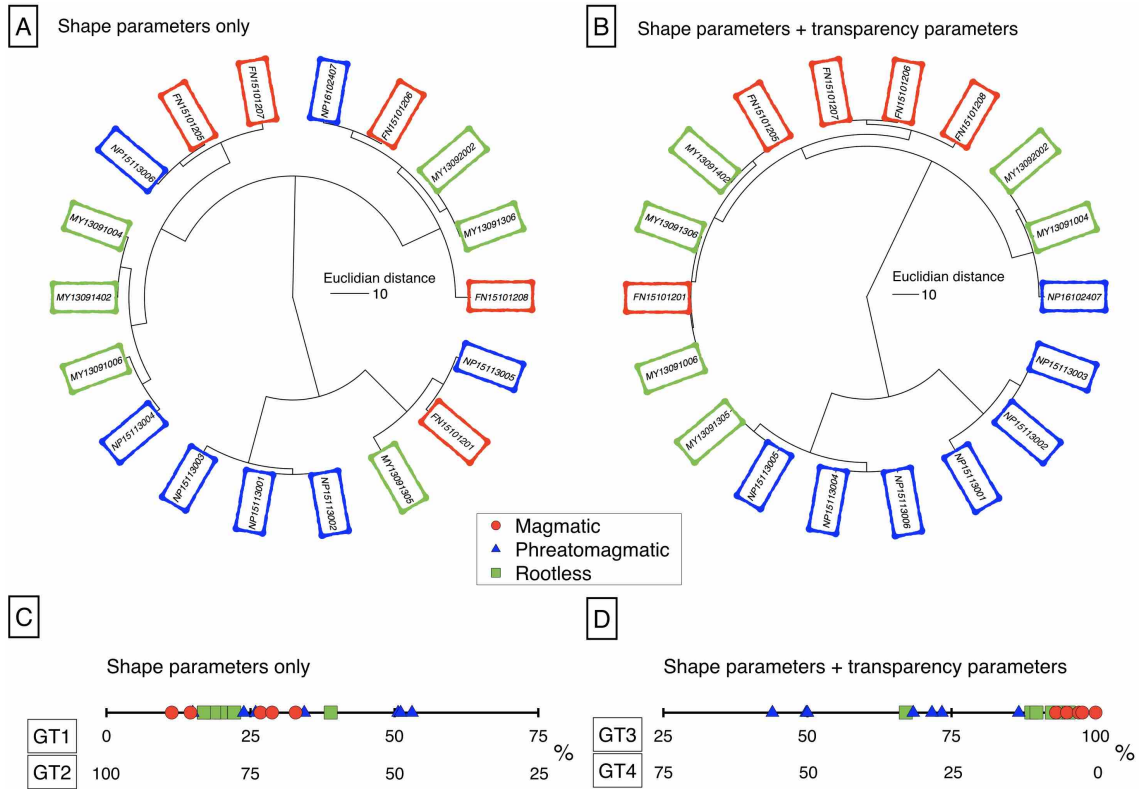


Figure 11: Results of cluster analysis 2: sample clustering. A and C: grain types are determined based on shape parameters only and B and D: grain types are determined based on shape parameters and transparency values. Red, blue, and green boxes indicate magmatic, phreatomagmatic, and rootless samples, respectively. C and D: number lines for grain type percentages.

## 4 Discussion

### 4.1 Verification of introducing grain types by the cluster analysis

The components of the grain type in each sample are consistent with microscopic observations by human eyes. As noted in 2.1.2, we found two characteristics of grain shape: inwardly convex shape and rectilinear edge. This difference appeared in our grain types; inwardly convex shape grains corresponds GT1 and GT4, and rectilinear edge grains correspond GT2 and GT3, respectively. This difference effects to the sample clustering (Fig.11). In human eyes, transparent grains are dominant in MY13091004 and MY13091305, and opaque grains are dominant in MY13091006 and MY13091402. Our grain types which consider both of grain shape and transparency are consistent with this qualitative observation; MY13091004 and MY13091305 has higher contents of GT4 grains, and MY13091006 and MY13091402 has significantly higher contents of GT3 grains (Table 3). However, FN15101206, has higher component of brownish yellow grains in microscopic observations, did not show unique grain type component in our analysis. Possibly, these brownish yellow grains might be appeared as opaque on Morphologi images.

We have clarified that grain transparency plays an important role in the classification of grain and sample types. Previous studies have considered only grain shape, ignoring the transparency of grains, with the exception of [Miwa et al., 2015]. The identification of transparent grains is important for detecting juvenile glass fragments; however, in this study, as the recommended number of grain types was two, all transparent grains were analyzed together, i.e., it was impossible to distinguish between glass fragments and transparent free-crystals, and between sideromelane and tachylite. Glass fragments considered to formed by two quenching processes: air-cooling and magma (lava) external water interaction. Therefore amount of glass fragments is expected to be larger in phreatomagmatic and rootless eruptions (both of air-cooling and magma (lava) external water interaction) than those of magmatic eruptions (air-cooling only).

295 Generation of free-crystals is thought to dependent on the degree of fragmentation;  
296 stronger explosion generates larger numbers of free-crystals. Assuming same mode, assem-  
297 blage, and size of phenocryst in host magma (lava), phreatomagmatic eruptions might be  
298 generating larger numbers of free-crystals than the others. Thus, GT4 in the cluster analy-  
299 sis with transparency would be mixture of glass fragments and transparent free-crystals by  
300 mechanisms shown above. Hence this explains difference of the GT3/GT4 among eruption  
301 types.

302 In the next stage we should explore an efficient criteria to distinguish glass from phe-  
303 nocryst. For example, quenching of magma (lava) by external water would likely gener-  
304 ate a larger amount of sideromelane fragments (e.g., [Taddeucci et al., 2004]). Therefore,  
305 identification of sideromelane fragments would be an effective way to discriminate between  
306 phreatomagmatic and magmatic samples. Performing the clustering procedure with a larger  
307 number of grain types might enable us to distinguish whether glass fragments are siderome-  
308 lane or tachylite. In our ash grain images, it is possible to identify microlites inside of some  
309 transparent grains (Fig.12). Microlites in glass grains are thought to decrease transparency  
310 of ash grains. Furthermore, oxidization and existence of microbubbles are also expected  
311 to increase opacity of ash grains (e.g., [Yamanoi et al., 2008]; [Mujin and Nakamura, 2014];  
312 [Toramaru, 1990]). Hence these controls on the transparency of ash grains should be exam-  
313 ined under SEM (Scanning Electron Microscope) observations as a next step.

## 314 **4.2 Applicability to identification of explosion/fragmentation pro-** 315 **cess**

316 By incorporating transparency values into the grain type determination, Funabara (formed  
317 by magmatic eruption) and Nippana (formed by phreatomagmatic eruption) samples were  
318 clearly distinguished (Fig. 11A). The decisive factor is the amount of GT4 grains; it is less  
319 than 7 % for Funabara samples and up to 56 % for Nippana samples. GT4 grains show sig-  
320 nificant transparency and irregular shape features (Fig. 8), which might represent quenched

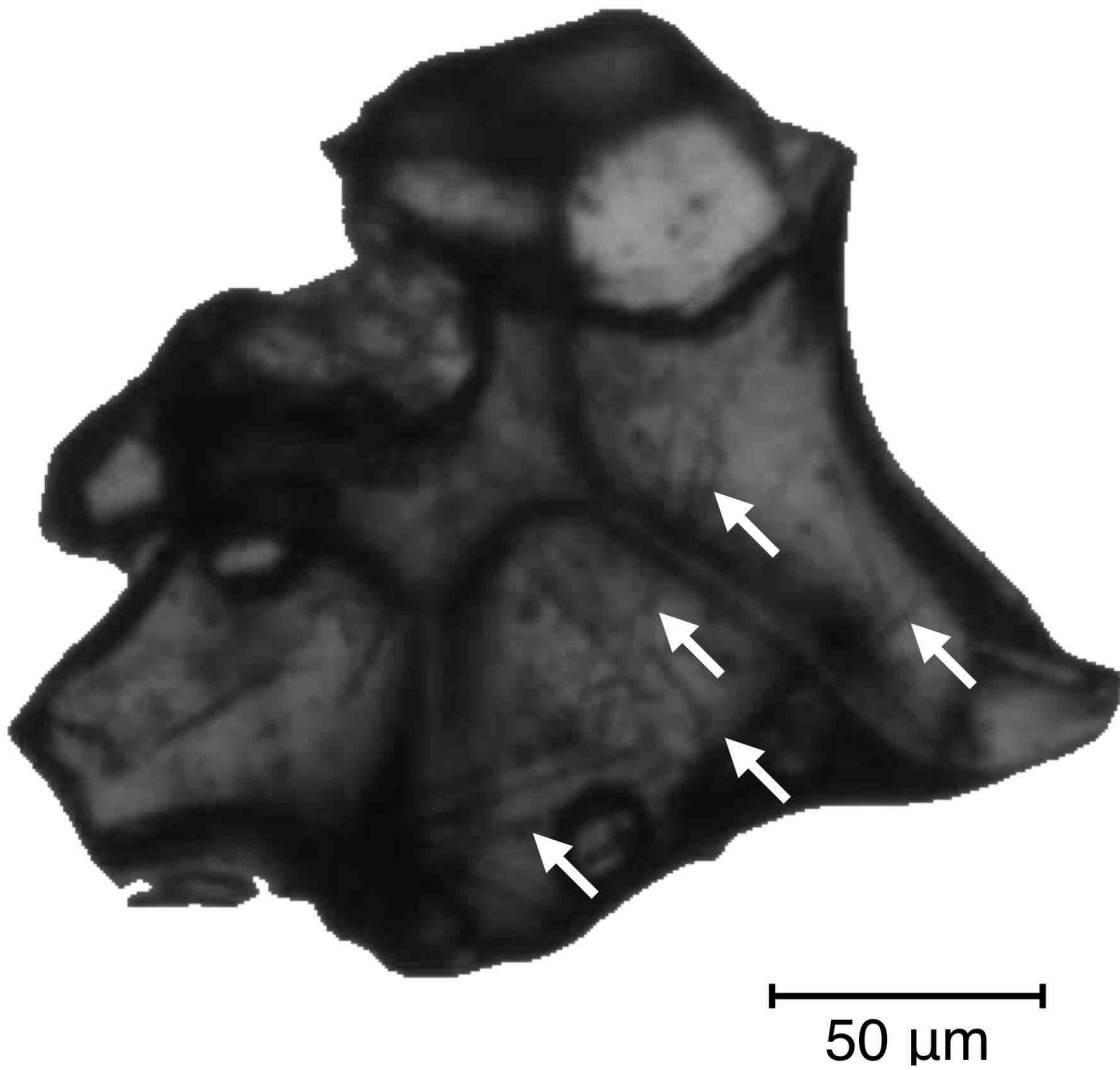


Figure 12: An example transparent grain which contains microlites (elongated obstacles, possible plagioclase, white arrows).

321 glass such as sideromelane. Therefore, in this clustering scheme, GT4 percentages could be  
322 used to infer the magnitude of the effect of external water on volcanic explosions (Fig. 11D).  
323 A smaller scale cluster structure indicates a possible variation in eruption/fragmentation  
324 styles and mechanisms during a volcanic eruption. For example, Funabara samples were sep-  
325 arated consistent with its stratigraphy (lower layers: FN15101201 and FN15101205, upper  
326 layers: FN15101206, FN15101207, and FN15101208) (Fig. 11B). Lower–middle layers of Nip-  
327 pana samples were also separated consistent with its stratigraphy (lower layers: NP15113001,  
328 NP15113002 and NP15113003, middle layers: NP15113004, NP15113005, and NP15113006).  
329 NP16102407 is collected from an upper layer, and distinguished from lower samples. How-  
330 ever, samples from magmatic and rootless eruptions were not completely separated from one  
331 another, and one rootless sample (MY13091305) was categorized with the phreatomagmatic  
332 samples. This means the boundary between rootless eruption and phreatomagmatic eruption  
333 is obscure. The highly variable clustering of rootless samples indicates strong variations in  
334 the explosion style (e.g., [Fagents and Thordarson, 2007]; [White and Valentine, 2016]).

335 Our sample classification may be able to extract and distinguish explosion (fragmentation)  
336 processes. It can be possible to simplified explosion (fragmentation) process into two; the  
337 vaporization of volatiles originally contained in magma, and the magma (lava)-water inter-  
338 action analogized as the molten fuel-coolant interaction (MFCI) (e.g., [Dellino et al., 2001]).  
339 For example, cluster of NP15113001, NP15113002 and NP15113003 may be represent explo-  
340 sive phase of phreatomagmatic explosions which are driven by both of volatile vaporizations  
341 and MFCIs. In contrast, cluster of NP15113004, NP15113005, and NP15113006 may show  
342 subsequent weaken phase of phreatomagmatic explosions which are driven by MFCIs domi-  
343 nantly (volatiles have been degassed, possibly). This explosion process probably significant in  
344 generations of NP16102707, MY13091004, and MY13092002. FN15101206, FN15101207, and  
345 FN15101208 might be formed by mostly pure volatile vaporization-driven explosions. Though  
346 we could not distinguish the other samples which not shown above, these samples might were  
347 formed by subequal degree of fragmentation in fine balances of volatile vaporizations and

348 MFCIs (and perhaps other processes), which may be able to distinguish in further analy-  
349 ses. Thus, our classification method will be contribute to extract explosion/fragmentation  
350 processes from volcanic ash grain data.

### 351 **4.3 Development of this procedure in volcanology and other fields**

352 In this study, we show that using grain transparency as well as grain shape significantly  
353 improves the result of the cluster analysis for volcanic ash grains. Our two-step cluster  
354 analysis enabled the comparison of many volcanological samples consisting of thousands of  
355 ash grains. The merit of our procedure is that it can be used for volcanic ash analysis  
356 of different outcrops, volcanoes, and eruption styles. However, to apply this procedure to  
357 volcanic ash from non-basaltic and non-monogenetic volcanoes, the effects of different magma  
358 compositions and alteration degrees should first be verified.

359 The estimation of an appropriate cluster number depends on each clustering method.  
360 In this study, we adopted the Ward method because of its popularity. It is our important  
361 future work to use other clustering algorithms developed in machine learning community  
362 ([Gokcay and Principe, 2002]; [Hino and Murata, 2014]) to obtain detailed characteristics of  
363 grain types.

364 Furthermore, machine learning techniques would be required to apply the results of our  
365 analyses to other ash samples. Involving our classified volcanic ash images as training data  
366 in the supervised learning, machine can identify grains and samples. For this application,  
367 further grain parameters (e.g., RGB (red, green, and blue) color under the incident lighting  
368 which have information about oxidization and alteration) and further types of samples (e.g.,  
369 collected from non-monogenetic, non-basaltic volcanoes).

370 Although our analyses show the importance of transparency in the clustering of volcanic  
371 ash grains, it is not clear whether the average ( $I_m$ ) and standard deviation ( $I_{sd}$ ) of gray scale  
372 values of one grain are sufficient for accurate identification. For instance, [Liu et al., 2015]  
373 showed that the choice of parameters plays a significant role in statistical analysis. Despite

374 parameter limitations, the machine learning technique is expected to be useful for direct  
375 volcanic ash image interpretation ([Shoji and Noguchi, 2017]).

376 The development of our procedure will be useful outside volcanology, such as sedimen-  
377 trolgy and planetary science (e.g., sample return mission such as for Mars and asteroids).

## 378 **5 Conclusions**

379 We constructed a statistical procedure for comparing volcanic ash samples from several out-  
380 crops and volcanoes. Using the cluster analysis, we set "grain types", then categorized  
381 samples by its components of each grain type. Testing our data set, we found that grain  
382 types should be two, and the transparency values of grains is effective to categorize sam-  
383 ples consistent with their origins. This procedure detailed in this study could be used to  
384 interpret changes in eruption/fragmentation style during a volcanic event. Through further  
385 analyses and using other machine learning techniques, our procedure can contribute outside  
386 volcanology and Earth.

## 387 **Acknowledgements**

388 Grain data in this study were collected using Morphologi G3S at the Geological Survey  
389 of Japan, AIST. Discussion with Hiroaki Sato and Daigo Shoji was helpful to considering  
390 transparency of ash grains. We would like to acknowledge Yusuke Suzuki for help with  
391 the field work in the Izu Peninsula, the Tachiiwa corporation, a quarrying company of the  
392 Funabara scoria cone, for enabling sampling, Karóly Németh for field work assistance in  
393 Miyakejima, and Ármann Höskuldsson, Árni Einarsson, Eirik Gjarlow, Árni Fridriksson, and  
394 Tomotaka Saruya, who assisted R.N. and K.K. in the field work in Myvatn. The field work in  
395 Izu Peninsula and Iceland was funded by the Izu Peninsula Geopark Promotion Council and  
396 the Sasakawa Scientific Research Grant from The Japan Science Society for R.N. (25-602),  
397 respectively. H.H. is supported by KAKENHI No.16H02842, and JST CREST ACA20935.

398 This study was supported by the Joint Usage/ Research Center program No. 2015-B-04 from  
 399 the Earthquake Research Institute, the University of Tokyo, and KEKENHI No.17H02063.

400 **Appendix: in the case of three grain types**

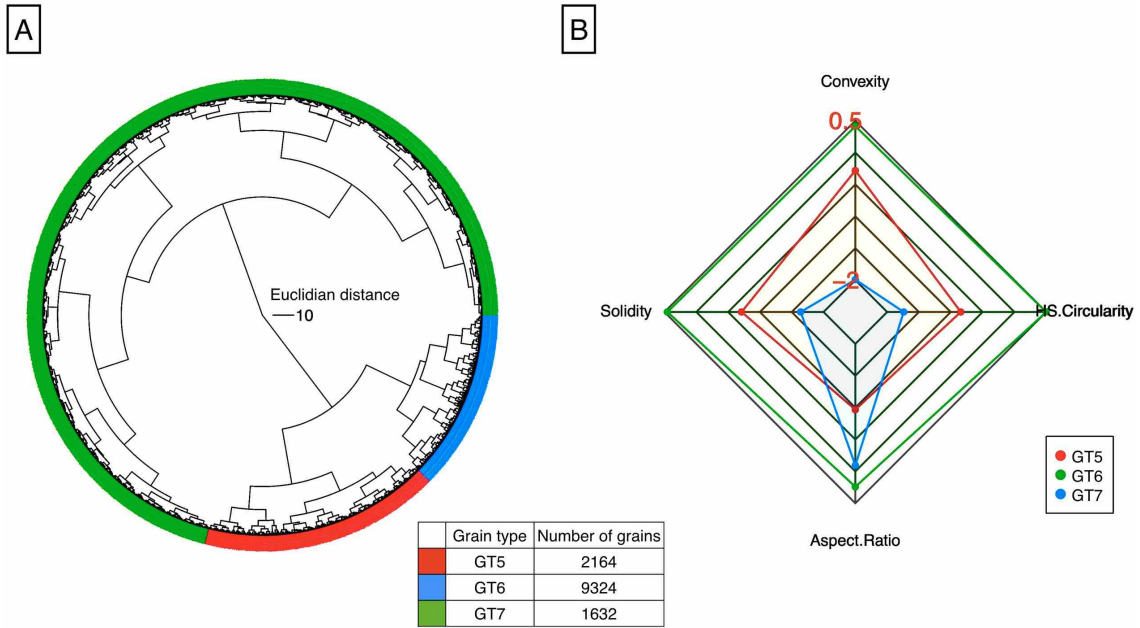


Figure 13: Results of cluster analysis 1: grain type determination. A : dendrogram for each grain type, and D: radar chart for each grain type.



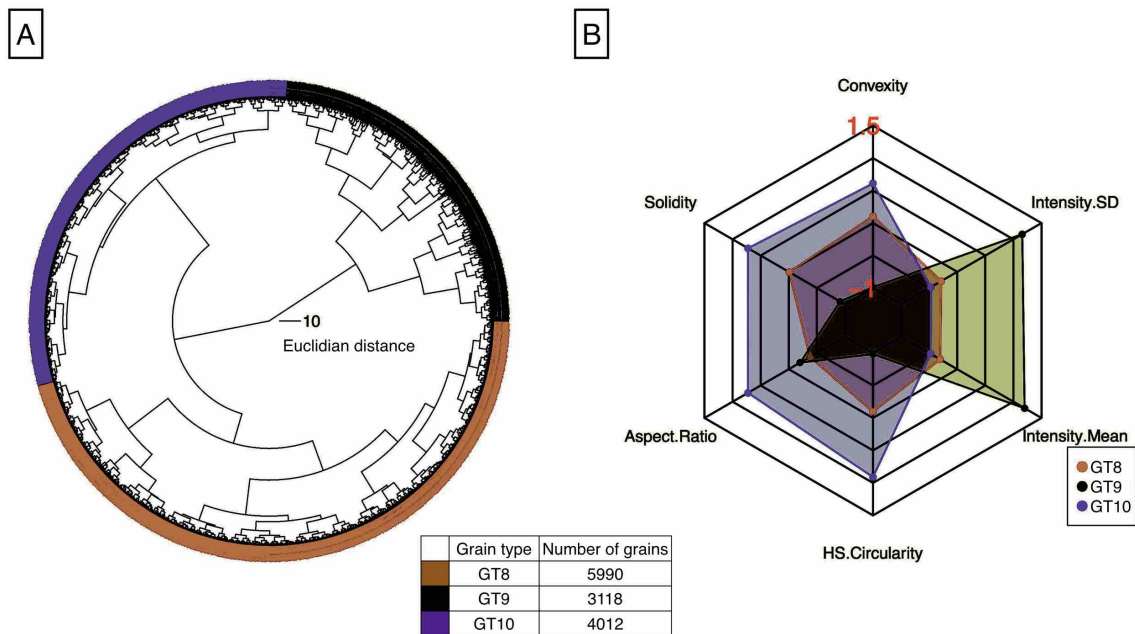


Figure 14: Results of cluster analysis 1: grain type determination. A : dendrogram for each grain type, and D: radar chart for each grain type.

## References

- 401
- 402 Anderberg, 2014. Anderberg, M. R., 2014, Cluster analysis for applications: probability and  
 403 mathematical statistics: a series of monographs and textbooks (Vol. 19), Academic press,  
 404 376 p.
- 405 Aramaki et al., 1986. Aramaki, S., Y. Hayakawa, T. Fujii, K. Nakamura, and T. Fukuoka,  
 406 1986, The October 1983 eruption of Miyakejima volcano, *J. Volcanol. Geotherm. Res.*,  
 407 **29**(1–4), 203–229.
- 408 Charrad et al., 2014. Charrad M., N. Ghazzali, V. Boiteau, and A. Niknafs, 2014, NbClust:  
 409 An R Package for Determining the Relevant Number of Clusters in a Data Set, *J. Statistical  
 410 Software*, **61**(6), 1–36, <http://www.jstatsoft.org/v61/i06/>.
- 411 Dellino and La Volpe, 1996. Dellino, P. and L. La Volpe., 1996, Image processing analysis in  
 412 reconstructing fragmentation and transportation mechanisms of pyroclastic deposits. The

Table 4: Grain type percentages for each sample in the case of grain types are three.

Sample ID	GT5 [%]	GT6 [%]	GT7 [%]	GT8 [%]	GT9 [%]	GT10 [%]
FN15101201	22.14	67.18	10.69	67.18	6.87	25.95
FN15101205	17.18	73.28	9.54	61.83	4.96	33.21
FN15101206	8.74	85.44	5.83	57.28	2.91	39.81
FN15101207	22.99	71.26	5.75	71.26	2.30	26.44
FN15101208	11.31	88.69	0.00	50.00	0.00	50.00
NP15113001	21.34	49.38	29.28	31.23	56.08	12.70
NP15113002	23.90	48.94	27.16	36.92	50.21	12.87
NP15113003	28.97	46.96	24.07	41.59	50.00	8.41
NP15113004	15.91	76.18	7.91	44.71	26.67	28.62
NP15113005	18.93	65.68	15.40	45.90	31.64	22.46
NP15113006	16.58	74.12	9.30	45.98	28.39	25.63
NP16102407	11.12	85.05	3.82	44.96	13.33	41.71
MY13091004	13.87	80.17	5.96	49.08	11.16	39.76
MY13091006	15.49	77.84	6.67	55.40	6.38	38.22
MY13091305	20.70	61.08	18.22	40.23	32.94	26.82
MY13091306	11.94	83.13	4.93	48.51	7.61	43.88
MY13091402	11.83	81.34	6.83	50.51	4.67	44.83
MY13092002	11.81	83.11	5.08	50.36	10.26	39.38

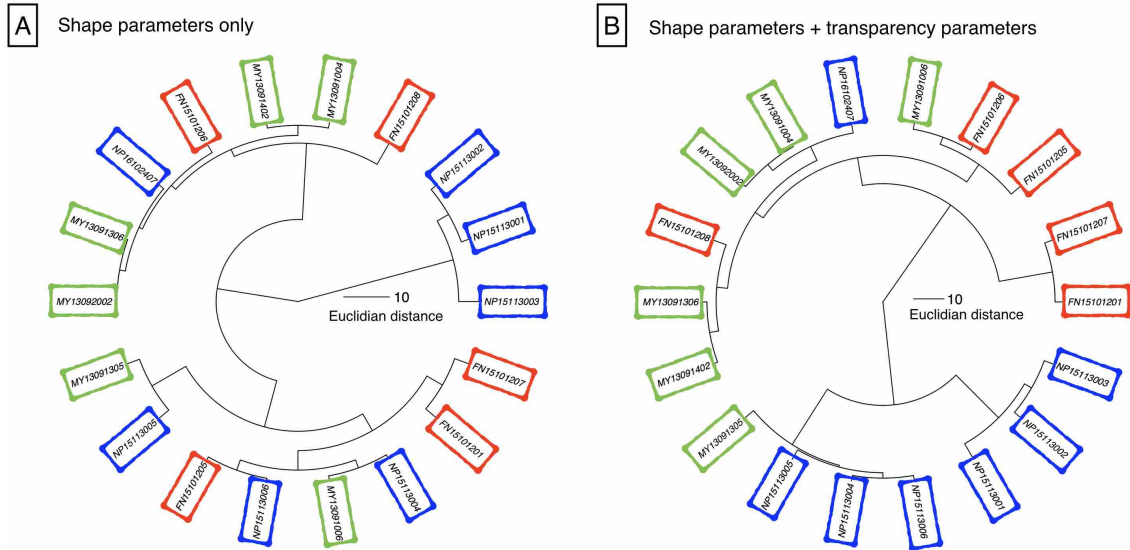


Figure 15: Results of cluster analysis 2: sample clustering for in the case of three grain types. A: grain types are determined based on shape parameters only, and B: grain types are determined based on shape parameters and transparency values. Red, blue, and green boxes indicate magmatic, phreatomagmatic, and rootless samples, respectively.

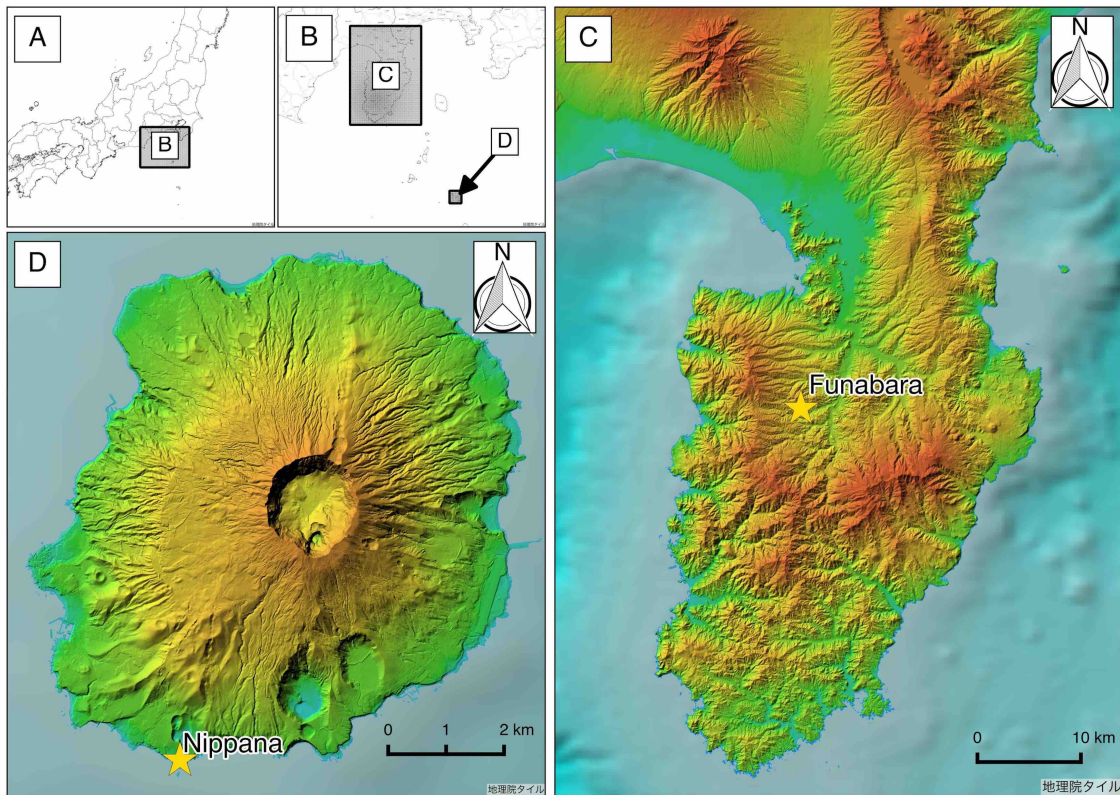


Figure S1: Sampling locations for Funabara scoria cone and Nippana tuff ring. This map is based on "Chiriin Tile" (<http://maps.gsi.go.jp>) of Geospatial Information Authority of Japan and Hydrographic and Oceanographic Department, Japan Coast Guard.

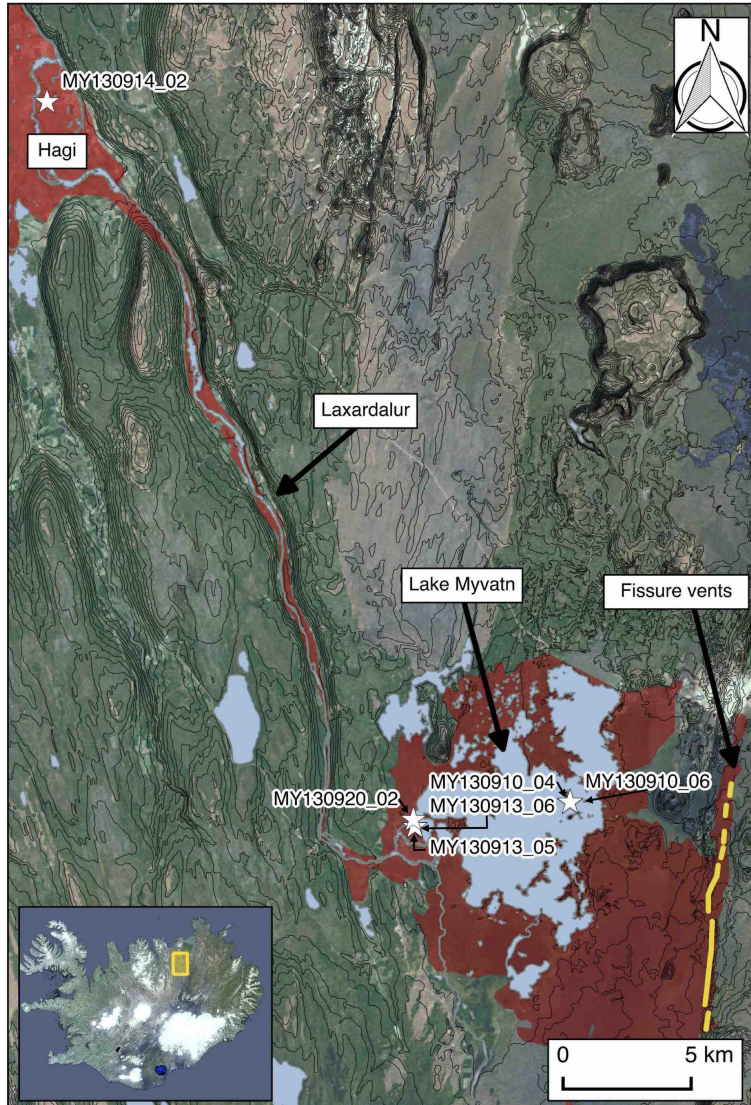


Figure S2: Sampling locations for rootless cones in Myvatn, Iceland. Red region shows extent of the Younger Laxá lava. Yellow lines show fissure vents. Black tiny lines show 10 m interval topographic contour lines based on the elevation model of Landmælingar Íslands (LMI). Background image is the Landsat image mosaic in natural colors (B,G,R), 30 m resolution. This map is based on data from National Land Survey of Iceland (NLSI).



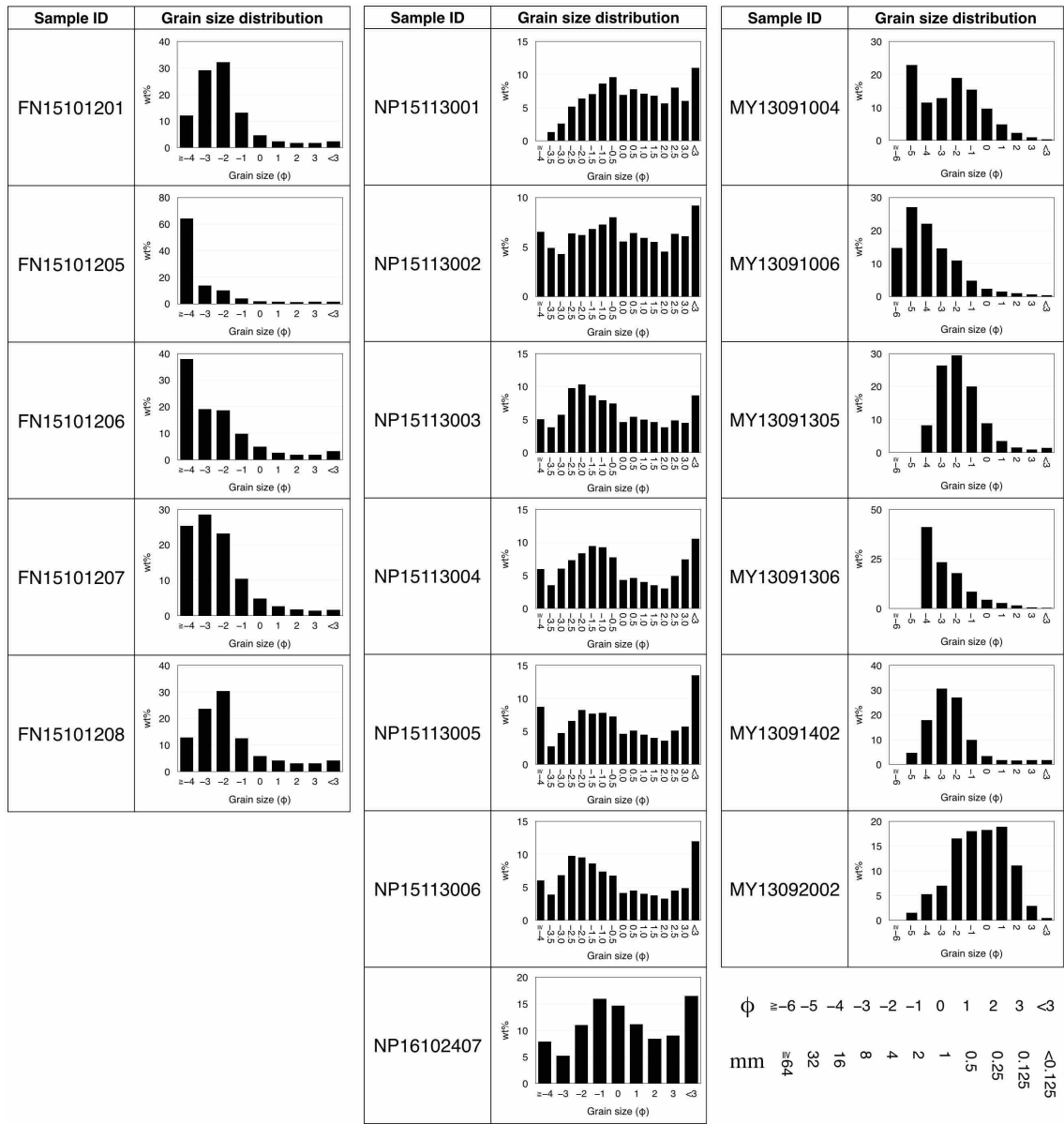


Figure S3: The grain size distribution of each sample.

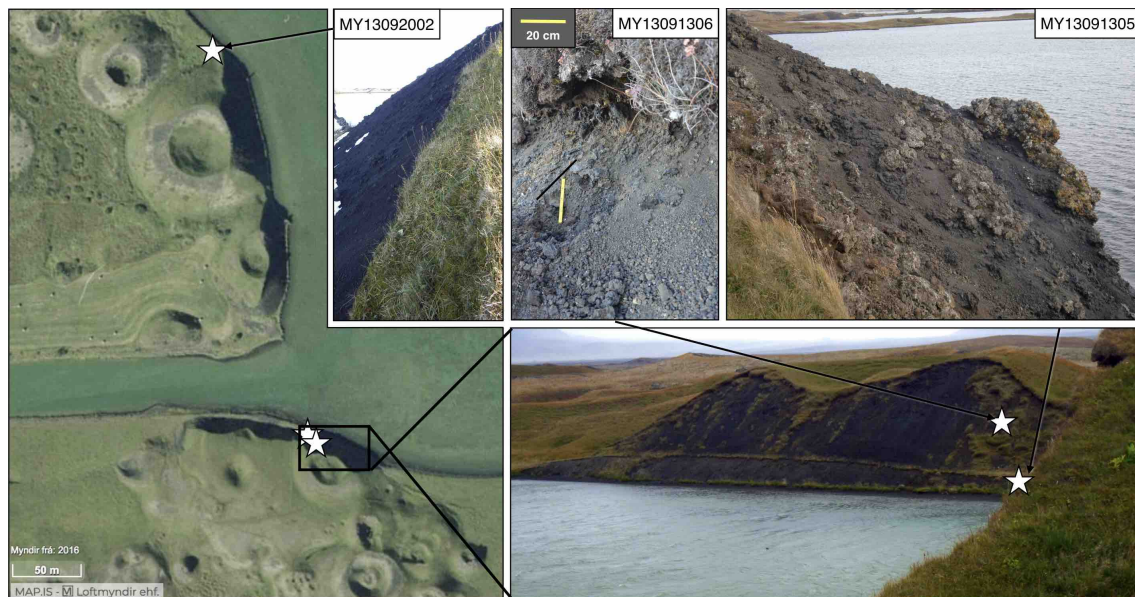


Figure S4: Sampling outcrops of Myvatn rootless cones.



Figure S5: Sampling outcrops of Myvatn rootless cones.

413 case of Monte Pilato-Rocche Rosse eruptions, Lipari (Aeolian islands, Italy), *J. Volcanol.*  
414 *Geotherm. Res.*, **71**, (1), 13–29.

415 Dellino et al., 2001. Dellino, P., R. Isaia, L. La Volpe, and G. Orsi, 2001, Statistical anal-  
416 ysis of textural data from complex pyroclastic sequences: implications for fragmentation  
417 processes of the Agnano-Monte Spina Tephra (4.1 áka), Phlegraean Fields, southern Italy,  
418 *Bull. Volcanol.*, **63**, (7), 443–461.

419 Dolvik, 2007a. Dolvik, T., 2007, Comparison of tephra from a crater row, pseudocraters and  
420 tephra fall-out, all tephra from a large effusive eruption, the Threngslaborgir-Lútentsborgir  
421 eruption 2300 BP in Mývatn, N-Iceland, *Geophys. Res. Abstracts*, 05513 p.

422 Dolvik, 2007b. Dolvik, T., Á. Höskuldsson, and P.V. Kolka, 2007, Comparison of tephra  
423 from a crater row and pseudocraters and tephra fall-out, all tephra from a large effusive  
424 eruptions, the Threngslaborgir - Lútentsborgir eruption 2300 BP in Mývatn, N-Iceland,  
425 *Vorrádstefna Jarðfræðafélags Íslands, Ágrip erinda*, 15 p.

426 Einarsson, 1982. Einarsson, Á., 1982, The palaeolimnology of Lake Mývatn, northern Ice-  
427 land: plant and animal microfossils in the sediment, *Freshwater Biology*, **12**, 63–82,  
428 doi:10.1111/j.1365-2427.1982.tb00603.x.

429 Fagents and Thordarson, 2007. Fagents, S.A. and T. Thordarson, 2007, Rootless volcanic  
430 cones in Iceland and on Mars, In: *The Geology of Mars, Cambridge University Press*,  
431 Cambridge, 151–177.

432 Fox, 2005. Fox, J., 2005, Getting started with the R commander: a basic-statistics graphical  
433 user interface to R, *J. of statistical software*, **14**, (9), 1–42.

434 Fujii et al., 1984. Fujii, T., S. Aramaki, T. Fukuoka, and T. Chiba, 1984, Petrology of the  
435 ejecta and lavas of the 1983 eruption of Miyake-jima, *Bull. Volc. Society of Japan*, **2**, (29),  
436 266–282 (in Japanese with English abstract).

- 437 Gokcay and Principe, 2002. Gokcay, E. and J. Principe, 2002, Information Theoretic Clus-  
438 tering, *IEEE Transactions on Pattern Analysis and Machine Intelligence*, **24**(2) , 158–170.
- 439 Gonnermann, 2015. Gonnermann, H.M., 2015, Magma fragmentation, *Annual Rev. of Earth*  
440 *and Planet. Sci.*, **43** , 431–458.
- 441 Hamuro, 1985. Hamuro, K., 1985, Petrology of the Higashi-Izu Monogenetic Volcano Group,  
442 *Bull. the Earthquake Res. Inst.*, University of Tokyo, **60**, 335–400.
- 443 Hasebe et al., 2001. Hasebe, N., A. Fukutani, M. Sudo, and T. Tagami, 2001, Transition of  
444 eruptive style in an arc–arc collision zone: K–Ar dating of Quaternary monogenetic and  
445 polygenetic volcanoes in the Higashi-Izu region, Izu peninsula, Japan, *Bull. Volcanol.*, **63**,  
446 377–386.
- 447 Hauptfleisch, 2012. Hauptfleisch, U., 2012, High-resolution palaeolimnology of Lake Mývatn,  
448 Iceland, *PhD thesis of University of Iceland* , Reykjavik.
- 449 Heiken and Wohletz, 1985. Heiken, G. and K. Wohletz, 1985, Volcanic ash, University  
450 Presses of California, Chicago, Harvard & MIT, 246 p.
- 451 Nicholson, 1990. Nicholson, H., 1990, The magmatic evolution of Krafla, NE Iceland, *PhD*  
452 *thesis of Edinburgh University* , Edinburgh.
- 453 Hino and Murata, 2014. Hino, H. and N. Murata, 2014, A Non-parametric Clustering Algo-  
454 rithm With A Quantile-based Likelihood Estimator, *Neural Computation*, **26**, (9), 2074–  
455 2101.
- 456 Hon et al., 1994. Hon, K., L. Kauahikaua, R. Denlinger, and K. Mackay, 1994, Emplacement  
457 and inflation of pahoehoe sheet flows: observations and measurements of active lava flows  
458 on Kilauea Volcano, Hawaii, *Geol. Society of America Bull.*, **106**, (3), 351–370.



459 Höskuldsson et al., 2010. Höskuldsson, Á., C. Dyhr, and T. Dolvik, 2010, Grænavatnsbruni  
460 og Laxárhraun yngra, *Haustrá dsteftna Jarðfræðafélags Íslands, Ágrip erinda*, 41–44 (in  
461 Icelandic).

462 Koyama and Umino, 1991. Koyama, M. and S. Umino, 1991, Why Does the Higashi-Izu  
463 Monogenetic Volcano Group Exist in the Izu Peninsula?, *J. Phys. Earth*, **39.1**, 391–420.

464 Kueppers et al., 2006. Kueppers, U., D. Perugini, and D.B. Dingwell, 2006, ???Explosive  
465 energy??? during volcanic eruptions from fractal analysis of pyroclasts, *Earth and Planet.*  
466 *Sci. Lett.*, **248**, (3): 800–807.

467 Leibbrandt and Le Pennec, 2015. Leibbrandt, S., and J.L. Le Pennec, 2015, Towards fast and  
468 routine analyses of volcanic ash morphometry for eruption surveillance applications, *J.*  
469 *Volcanol. Geotherm. Res.*, **297**, 11–27.

470 Liu et al., 2015. Liu, E.J., K.V. Cashman, and A.C. Rust, 2015, Optimising shape analysis  
471 to quantify volcanic ash morphology, *GeoResJ*, **8**, 14–30.

472 Malvern Instruments Ltd, 2013. Malvern Instruments Ltd, 2013, Morphologi G3 User Man-  
473 ual, *GeoResJ*, **8**, 280 p.

474 Maria and Carey, 2002. Maria, A., and S. Carey, 2002, Using fractal analysis to quantita-  
475 tively characterize the shapes of volcanic particles, *J. Geophys. Res.*, **107**, B11.

476 Maria and Carey, 2007. Maria, A., and S. Carey, 2007, Quantitative discrimination of  
477 magma fragmentation and pyroclastic transport processes using the fractal spectrum tech-  
478 nique, *J. Volcanol. Geotherm. Res.*, **161**, 234–246.

479 Miwa et al., 2015. Miwa, T., T. Shimano, and T. Nishimura, 2015, Characterization of the  
480 luminance and shape of ash particles at Sakurajima volcano, Japan, using CCD camera  
481 images, *Bull. Volcanol.*, **77**(1), 5.

482 Mujin and Nakamura, 2014. Mujin, M. and M. Nakamura, 2014, A nanolite record of erup-  
483 tion style transition, *Geology*, **42**(7), 611–614.

484 Noguchi et al., 2016. Noguchi, R., Á. Höskuldsson, and K. Kurita, 2016, Detailed topograph-  
485 ical, distributional, and material analyses of rootless cones in Myvatn, Iceland. *J. Volcanol.*  
486 *Geotherm. Res.*, **318**, 89–102.

487 Rausch et al., 2015. Rausch, J., B. Grobéty, and P. Vonlanthen, 2015, Eifel maars: Quan-  
488 titative shape characterization of juvenile ash particles (Eifel Volcanic Field, Germany) *J.*  
489 *Volcanol. Geotherm. Res.*, **291**, 86–100.

490 R Core Team, 2016. R Core Team, 2016, R: A language and environment for statistical com-  
491 puting, *R Foundation for Statistical Computing*, Vienna, Austria. URL [https://www.R-](https://www.R-project.org/)  
492 [project.org/](https://www.R-project.org/).

493 Reynolds et al., 2015. Reynolds, P., R.J. Brown, T. Thordarson, E.W. Llewelin, and K.  
494 Fielding, 2015, Rootless cone eruption processes informed by dissected tephra deposits and  
495 conduits, *Bull. Volcanol.*, **77**, (9), 1–17.

496 Schmith et al., 2017. Schmith, J., Á. Höskuldsson, and P.M. Holm, 2017, Grain shape of  
497 basaltic ash populations: implications for fragmentation, *Bull. Volcanol.*, **79**, (2), 14.

498 Sheridan and Wohletz, 1983. Sheridan, M.F. and K.H. Wohletz, 1983, Hydrovolcanism: ba-  
499 sic considerations and review, *J. Volcanol. Geotherm. Res.*, **17**, (1), 1–29.

500 Shoji and Noguchi, 2017. Shoji, D. and R. Noguchi, 2017, Shape recognition of volcanic ash  
501 by simple convolutional neural network, arXiv:1706.07178 [physics.geo-ph]

502 Sumita, 1985. Sumita, M., 1985, Ring-shaped cone formed during the 1983 Miyake-jima  
503 eruption, *Bull. Volcanol. Soc. Japan*, **30**, 11–32. in Japanese

504 Taddeucci et al., 2004. Taddeucci, J., M. Pompilio, and P. Scarlato, 2004, Conduit processes  
505 during the July–August 2001 explosive activity of Mt. Etna (Italy): inferences from glass

506 chemistry and crystal size distribution of ash particles, *J. Volcanol. Geotherm. Res.*, **131**,  
507 (1), 33–54.

508 Thorarinsson, 1953. Thorarinsson, S., 1953, The crater groups in Iceland, *Bull. vol-*  
509 *canologique*, **2**, 1–44.

510 Thorarinsson, 1979. Thorarinsson, S., 1979, The postglacial history of the Mývatn area,  
511 *Oikos*, **32**, 16–28.

512 Thordarson and Höskuldsson, 2002. Thordarson, T. and Á. Höskuldsson, 2002, Iceland,  
513 *Terra Publishing*, Edinburgh, 200 p.

514 Toramaru, 1990. Toramaru, A., 1990, Measurement of bubble size distributions in vesicu-  
515 lated rocks with implications for quantitative estimation of eruption processes, *J. Volcanol.*  
516 *Geotherm. Res.*, **43**, (1), 71–90.

517 Walker, 1971. Walker, G.P., 1971, Grain-Size Characteristics of Pyroclastic Deposits, *J. of*  
518 *Geol.*, **79**, 696–714.

519 White and Valentine, 2016. White, J.D. and G.A. Valentine, 2016, Magmatic versus  
520 phreatomagmatic fragmentation: Absence of evidence is not evidence of absence, *Geo-*  
521 *sphere*, **12**(5), 1478–1488.

522 Wohletz, 1983. Wohletz, K., 1983, Mechanisms of hydrovolcanic pyroclast formation: grain-  
523 size, scanning electron microscopy, and experimental studies, *J. Volcanol. Geotherm. Res.*,  
524 **17**, (1), 31–63.

525 Wohletz and Heiken. Wohletz, K. and G. Heiken, 1992, Volcanology and geothermal energy,  
526 *University of California Press*, Berkeley, 432 p.

527 Wohletz et al., 1989. Wohletz, K., M. Sheridan, and W. Brown, 1989, Particle size distribu-  
528 tions and the sequential fragmentation/transport theory applied to volcanic ash, *J. Geo-*  
529 *phys. Res.*, **94**, 15703–15721.

530 Yamanoi et al., 2008. Yamanoi, Y., S. Takeuchi, S. Okumura, S. Nakashima, and T.  
531 Yokoyama, 2008, Color measurements of volcanic ash deposits from three different styles  
532 of summit activity at Sakurajima volcano, Japan: Conduit processes recorded in color of  
533 volcanic ash, *J. Volcanol. Geotherm. Res.*, **178** (1), 81–93.

534 Yusa and Kuroda, 1970. Yusa, Y. and N. Kuroda, 1970, Geology and petrology of Izu-  
535 Takatsukayama and Funabara volcano, *Geoscience reports of Shizuoka Univ.*, **2**(1), 43–54  
536 (In Japanese).\*

537 Zimanowski et al., 2003. Zimanowski, B., K. Wohletz, P. Dellino, and R. Büttner, 2003, The  
538 volcanic ash problem, *J. Volcanol. Geotherm. Res.*, **122**, 1–5.

539 \*Title etc. translated by R.N.